Unified treatment of hadronic annihilation and protonium formation in slow collisions of antiprotons with hydrogen atoms

Kazuhiro Sakimoto
Institute of Space and Astronautical Science, Japan Aerospace Exploration Agency, Yoshinodai 3-1-1, Chuo-ku, Sagamihara 252-5210, Japan
(Received 9 April 2013; published 12 July 2013)

Antiproton ($\bar{p}$) collisions with hydrogen atoms, resulting in the hadronic process of particle-antiparticle annihilation and the atomic process of protonium ($\bar{p}p$) formation (or $\bar{p}$ capture), are investigated theoretically. As the collision energy decreases, the collision time required for the $\bar{p}$ capture becomes necessarily longer. Then, there is the possibility that the $\bar{p}$-p annihilation occurs significantly before the $\bar{p}$ capture process completes. In such a case, one can no longer consider the annihilation decay separately from the $\bar{p}$ capture process. The present study develops a rigorous unified quantum-mechanical treatment of the annihilation and $\bar{p}$ capture processes. For this purpose, an R-matrix approach for atomic collisions is extended to have complex-valued R-matrix elements allowing for the hadronic annihilation. Detailed calculations are carried out at low collision energies ranging from 10^{-8} to 10^{-1} eV, and the annihilation and the $\bar{p}$ capture (total and product-state selected) cross sections are reported. Consideration is given to the difference between the direct annihilation occurring during the collision and the annihilation of $\bar{p}p$ occurring after the $\bar{p}$ capture. The present annihilation process is also compared with the annihilation in two-body $\bar{p} + p$ collisions.

DOI: 10.1103/PhysRevA.88.012507 PACS number(s): 36.10.Gv, 25.43.+t, 34.50.Fa, 34.50.Lf

I. INTRODUCTION

When an antiproton $\bar{p}$ collides with a hydrogen H atom at collision energies $E_{\rm coll}$ less than the ionization threshold, two quite different types of reaction channels are of critical importance [1–3]. One is an atomic rearrangement process: the capture of $\bar{p}$ to form an exotic hydrogenic atom $\bar{p}p$ called antiprotonic hydrogen or protonium,

$$\bar{p} + \mathrm{H} \rightarrow \bar{p}p + e. \tag{1}$$

This $\bar{p}$ capture results in highly excited $\bar{p}p$ typically having the principal quantum number $N \sim \sqrt{m_p/(2m_e)} \simeq 30$, with the p mass m_p and the e mass m_e. The $\bar{p}p$ atoms cannot be permanently stable since the exotic system composed of a particle and its antiparticle has a finite lifetime against (pair) annihilation. As an atomic system, Eq. (1) is often characterized by the presence of the Fermi-Teller critical distance $R_{\rm FT} = 0.639$ a.u. [4]. If the $\bar{p}$-H distance R is less than $R_{\rm FT}$, no electronic bound state exists for a fixed R in this system. Owing to this fact, Eq. (1) usually has a very large cross section [5]. The other reaction channel is a hadronic decay process: the annihilation occurring just during the $\bar{p} + \mathrm{H}$ collisions,

$$\bar{p} + \mathrm{H} \rightarrow e + \bar{p}\text{-}p \text{ annihilation}. \tag{2}$$

In the present study, this *direct* annihilation is distinguished from the *indirect* annihilation which occurs after the $\bar{p}p$ atoms are formed by Eq. (1). The energy distribution of emitted electrons can be different for Eqs. (1) and (2); hence it may be possible to distinguish between the direct and indirect annihilation events in experiments by further measuring the electron energy distribution. Equation (2) is also an interesting decay process of $\bar{p}$ in matter to be compared with the annihilation in pure two-body (2B) collisions,

$$\bar{p} + p \rightarrow \text{annihilation}. \tag{3}$$

Because of the Coulomb attraction between $\bar{p}$ and p, the annihilation decays of Eqs. (2) and (3) can take place even at very low collision energies.

For an understanding of the significance of the direct annihilation occurring during the $\bar{p} + \mathrm{H}$ collision, it may be useful to compare the collision time of Eq. (1) with the annihilation lifetime of isolated $\bar{p}p$ atoms. The shifts and widths of some lowest $\bar{p}p$ energy levels due to the annihilation were determined by the measurement of x rays from $\bar{p}p$ atoms [1–3]. The annihilation width is $\Gamma_{1s} \sim 1$ keV for the $1s$ state, $\Gamma_{2p} \sim 40$ meV for the $2p$ state, and $\Gamma_{3d} \sim 0.4$ μeV for the $3d$ state. Thus, the annihilation lifetime of the s states becomes of major importance. The width Γ_{Ns} of the highly excited s level can be scaled as $N^{-3}\Gamma_{1s}$ [6]. If the principal quantum number $N = 30$ is considered, then the s-state lifetime is $\tau_{30s} \sim 2 \times 10^{-14}$ s. At low collision energies $E_{\rm coll} < 1$ eV, since the orbiting motion in polarization potential characterizes the ion-molecule reaction such as Eq. (1), the collision time may be estimated by $\tau_{\rm coll} = b_{\rm orb}/v$, with the orbiting impact parameter $b_{\rm orb}$ for the polarization force and the incident velocity v. Explicitly, this gives $\tau_{\rm coll} \simeq 10^{-14} \times [E_{\rm coll}(\mathrm{eV})]^{-3/4}$ s, which is comparable to or longer than τ_{30s} at $E_{\rm coll} \lesssim 0.1$ eV. It suggests that the annihilation is non-negligible at these energies as a decay process which occurs exactly in the course of the collision. It is now experimentally possible to cool many antiprotons in a trap to very low temperatures (<10 K) [7,8]. Cold collisions of antiprotons with atoms are an interesting subject in atomic and also nuclear physics.

Thus, it is necessary to devise a theoretical method of coherently taking account of both the atomic rearrangement and the $\bar{p}$-p annihilation channels in quantum-mechanical treatment, though the atomic and nuclear scales are quite different in space, time, and energy. Such efforts were made so far for low-energy $\mathrm{H} + \bar{\mathrm{H}}$ collisions [9–13], stimulated by recent progress on cold $\bar{\mathrm{H}}$ production [14–19]. To incorporate the $\bar{p}$-p annihilation into the atomic collision process,

Jonsell *et al.* [9] introduced a delta-function potential for the hadronic part of interaction, as well as usually applied to e^+-e annihilation. Voronin and Carbonell [10] and later Armour *et al.* [12] assumed an effective complex potential of the Woods-Saxon type [2] for the hadronic interaction. Jonsell *et al.* [11] considered the hadronic effect as a boundary condition of the wave function at a $\bar{p}$-p distance of ~ 1 a.u., and derived the hadronic information from experimental data of the $1s$ complex $\bar{p}p$ energy using the effective range theory known as the Trueman formula [20].

For the capture reaction of Eq. (1), although several quantum-mechanical calculations were carried out [21–24], no account of annihilation was taken in these studies. This is reasonable since high collision energies of $E_{\rm coll} \gtrsim 3$ eV were considered in most of them [22–24]. The purpose of the present study is to develop a unified and accurate treatment of Eqs. (1) and (2) by introducing an R-matrix methodology [25], in which the partitioning of the configuration space into appropriate domains is the favorite subject. Until now, the R-matrix method was employed for a rigorous treatment of an atomic process similar to Eq. (1), i.e., the capture of a negative muon (μ^-) by an H atom [26], in which the hadronic decay never occurs. The idea suggested by Jonsell *et al.* [11] can be properly incorporated in the R-matrix method by further inclusion of a domain providing hadronic information. In doing such extension, one can refer to several interesting R-matrix studies on atomic collisions [27–31]: The multipartitioning was introduced for solving the problems of chemical reaction and two-electron scattering. Since detailed information on the decay products in the $\bar{p}$-p annihilation is irrelevant, the annihilation is described by loss of a flux associated with the atomic channels. This is embodied by R-matrix elements having an imaginary part. In the present study, a new R-matrix treatment is developed for atomic collision processes allowing for annihilation decay. Accurate calculations are carried out for both the annihilation and the capture processes in $\bar{p}+{\rm H}$ at low collision energies ranging from 10^{-8} to 10^{-1} eV. The calculation is not limited to only s-wave scattering, and the partial waves of total angular momentum quantum numbers up to 17 are taken into account for determining the cross sections.

II. THEORY AND CALCULATIONS

Let $\mathbf{R}$ and $\mathbf{r}$ be the position vectors of $\bar{p}$ and e, respectively, measured from p. The configuration space is partitioned into several domains by the boundary lines $R = R_0, A, B$ and $r = b$, as seen in Fig. 1. Since the present problem covers a wide range of $\bar{p}$-p distances R from the nuclear size $R_0 \sim 10^{-5}$ a.u. to $\sim 10^3$ a.u., the R axis in Fig. 1 is drawn on a logarithmic scale. The annihilation can occur only at $R < R_0$. Outside the nuclear domain ($R > R_0$), the hadronic strong interaction is negligible, and the collision process is dominated by the Coulomb interaction

$$V = -\frac{1}{R} - \frac{1}{r} + \frac{1}{|\mathbf{R}-\mathbf{r}|}. \tag{4}$$

The outer $r \gtrsim b$ domain is associated with the $e+\bar{p}p$ arrangement, and the $R \gtrsim B$ domain is associated with the $\bar{p}+{\rm H}$ arrangement. The distance $R = B$ should be taken much larger than the Fermi-Teller critical value $R_{\rm FT}$. In the domain of $r \gtrsim b$ and $R \gtrsim B$, the total wave function is assumed to have negligible amplitudes. Specifically, $b = 8$ a.u. and $B = 2.7$ a.u. were chosen. The domain $\mathfrak{d}$ is defined by $R \in (R_0, A)$ and $r \in (0, b)$. It is convenient to choose the distance A as small as possible ($A = 1 \times 10^{-4}$ a.u. in the present calculation). Then, the probability of finding the electron at distances $r \leqslant A$ is negligibly small ($\sim 10^{-12}$). In the domain $\mathfrak{d}$, one can actually assume that $R \ll r$, and hence that the interaction is simply given by $V = -1/R$. The domain $\mathfrak{d}$ is introduced for working as a bridge from the nuclear domain to an atomic domain. The domain $\mathfrak{D}$ is defined by $R \in (A, B)$ and $r \in (0, b)$. The three-body (3B) correlation dynamics is limited largely to this domain. As shown in Fig. 1, the boundaries of the domains are denoted by $O_{\bar{p}}$, O_e, X, and I.

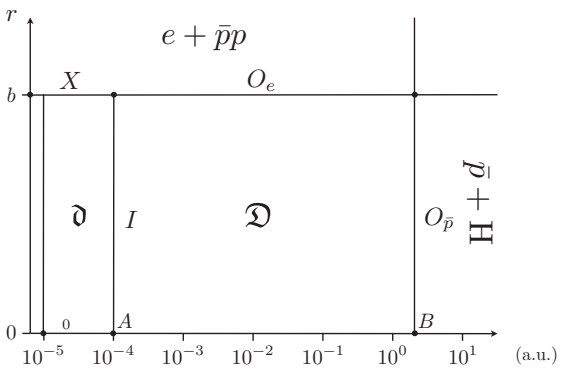

FIG. 1. Partitioning of the (R,r) configuration space by setting appropriate dividing lines $R = R_0, A, B$ and $r = b$. The R axis is drawn on a logarithmic scale. The outer domain $R \geqslant B$ or $r \geqslant b$: the arrangement channel $\bar{p}+{\rm H}$ or $e+\bar{p}p$ is defined. The nuclear domain $R \leqslant R_0$: the hadronic strong interaction dominates. The domain $\mathfrak{d}$: the Coulomb interaction $-1/R$ of $\bar{p}+p$ dominates. The domain $\mathfrak{D}$: the 3B correlation due to the Coulomb interaction is important. The boundaries of the partitioned domains are denoted by I ($R = A$), $O_{\bar{p}}$ ($R = B$), and $X + O_e$ ($r = b$).

In the present treatment, it is not necessary to provide an explicit form of the wave function representing the nuclear processes. Outside the nuclear domain ($R > R_0$), the time-independent Schrödinger equation is

$$(\mathsf{H} - E)\Psi^{JM}(\mathbf{R},\mathbf{r}) = 0, \tag{5}$$

with the total angular momentum quantum numbers (J,M), the total energy E, and the Hamiltonian H:

$$\mathsf{H} = -\frac{1}{2m_R}\frac{\partial^2}{\partial \mathbf{R}^2} - \frac{1}{2m_r}\frac{\partial^2}{\partial \mathbf{r}^2} + V, \tag{6}$$

where m_R and m_r are the reduced masses of $\bar{p}+p$ and $e+p$, respectively. Here and in the following, a.u. is used unless otherwise stated. The atomic problem is treated in the nonrelativistic framework. For the target of H atoms in the ground ($1s$) state, the total energy is $E = E_{\rm H} + E_{\rm coll}$, with $E_{\rm H} = -1/2$ and the $\bar{p}+{\rm H}$ collision energy $E_{\rm coll}$. In the coordinate system $(\mathbf{R},\mathbf{r})$, although the mass polarization term appears in the kinetic energy operators, Tong *et al.* [32] found that this term can be neglected in the $\bar{p}+{\rm H}$ system. In a previous R-matrix calculation, the present author had indicated that a mass polarization term was critical

for Feshbach-type resonances in $\bar{p}+\mathrm{He}^+$ [33]. However, Tong *et al.* confirmed that this term is insignificant also in the $\bar{p}+\mathrm{He}^+$ resonances. The reason for the discrepancy between the two studies is probably that the mass polarization term affects sensibly pseudoresonances (but not real resonances) which were not sufficiently eliminated from many existing resonances in the previous R-matrix calculation. The problem of pseudoresonances does not matter in the present calculation since no Feshbach resonances are involved. The neglect of the mass polarization term drastically lessens the labor in the numerical calculation.

A. Outer domain: Scattering channels

In the outer $r \gtrsim b$ domain, it is appropriate to expand the scattering wave function Ψ^{JM} using the basis set associated with the $e+\bar{p}p$ channel, i.e.,

$$\Psi^{JM}(\mathbf{r},\mathbf{R}) = (Rr)^{-1}\sum_{NLl}\mathcal{Y}^{JM}_{Ll}(\hat{\mathbf{R}},\hat{\mathbf{r}})\Upsilon_{NL}(R)f^{J}_{NLl}(r), \quad (7)$$

with $\Upsilon_{NL}(R)$ being the radial wave function of the $\bar{p}p$ bound state identified by the principal and angular momentum quantum numbers (N,L), and

$$\mathcal{Y}^{JM}_{Ll}(\hat{\mathbf{r}},\hat{\mathbf{R}}) = \sum_{m_l}(L,M-m_l,lm_l|JM)Y_{LM-m_l}(\hat{\mathbf{R}})Y_{lm_l}(\hat{\mathbf{r}}), \quad (8)$$

where $Y_{LM-m_l}(\hat{\mathbf{R}})$ and $Y_{lm_l}(\hat{\mathbf{r}})$ are the spherical harmonics, $(L,M-m_l,lm_l|JM)$ are the Clebsch-Gordan coefficients, l is the electronic angular momentum quantum number, and (J,M) are the total angular momentum quantum numbers. In the present case, the total parity must be $(-1)^{J+L+l}=1$. As will be shown later in Sec. II D, the annihilation effect of $\bar{p}$-p can be neglected in this domain. The energy of the $\bar{p}p$ atom is assumed to be hydrogenic, i.e., $E_N=-m_R/(2N^2)$.

In the outer $R \gtrsim B$ domain associated with the $\bar{p}+\mathrm{H}$ channel, the scattering wave function Ψ^{JM} can be given in the Born-Oppenheimer (BO) separation form [22,26]

$$\Psi^{JM}(\mathbf{R},\mathbf{r}) = (Rr)^{-1}\mathcal{D}^{J}_{M0}(\hat{\mathbf{R}})\chi_{1\sigma}(R;r,\theta)F^{J}_{1\sigma}(R), \quad (9)$$

with $\chi_{1\sigma}(R;r,\theta)$ being the wave function of the lowest (1σ) BO state of $\bar{p}+\mathrm{H}$, and

$$\mathcal{D}^{J}_{M\lambda}(\hat{\mathbf{R}}) = \left[\frac{2J+1}{16\pi^2(1+\delta_{\lambda,0})}\right]^{1/2}\left[D^{J}_{M\lambda}(\hat{\mathbf{R}})+(-1)^{\lambda}D^{J}_{M,-\lambda}(\hat{\mathbf{R}})\right]^{*}, \quad (10)$$

where $D^{J}_{M\lambda}(\hat{\mathbf{R}})$ is the Wigner rotation function, θ is the angle between $\mathbf{R}$ and $\mathbf{r}$, and λ is the electronic magnetic quantum number projected onto $\hat{\mathbf{R}}$. The accuracy of the BO approximation is guaranteed by the condition $B \gg R_{\mathrm{FT}}$. The wave function $F^{J}_{1\sigma}(R)$ represents the radial motion in the 1σ BO potential $V_{1\sigma}(R)$ [34]. In the present system, the scattering channels are identified by (N,L,l) or 1σ.

B. Domain $\mathfrak{d}$: Hadronic effects

In the domain $\mathfrak{d}$, since the interaction becomes $V=-1/R$, the $\mathbf{R}$ and $\mathbf{r}$ motions can be solved in separable form. Generally, the scattering wave function Ψ^{JM} in this domain is expressed as

$$\Psi^{JM}(\mathbf{R},\mathbf{r}) = (Rr)^{-1}\sum_{\nu Ll}\mathcal{Y}^{JM}_{Ll}(\hat{\mathbf{R}},\hat{\mathbf{r}})\xi_{\nu l}(r)G^{J}_{\nu Ll}(R), \quad (11)$$

where $\xi_{\nu l}(r)$ is the channel function [31] obtained from the Schrödinger equation including a Bloch operator [35]:

$$\left[-\frac{1}{2m_r}\frac{d^2}{dr^2}+\frac{l(l+1)}{2m_r r^2}+\frac{\delta(r-b)}{2m_r}\frac{d}{dr}-\epsilon_{\nu l}\right]\xi_{\nu l}(r)=0, \quad (12)$$

with the normalization

$$\int_0^b \xi_{\nu l}(r)\xi_{\nu' l}(r)dr = \delta_{\nu\nu'}. \quad (13)$$

The channels on the boundary I are given by (ν,L,l). What is important is that the function $G^{J}_{\nu Ll}(R)$ is determined by only the Coulomb potential $-1/R$, i.e.,

$$\left[-\frac{1}{2m_R}\frac{d^2}{dR^2}+\frac{L(L+1)}{2m_R R^2}-\frac{1}{R}-\frac{\kappa^2}{2m_R}\right]G^{J}_{\nu Ll}(R)=0, \quad (14)$$

with $\kappa^2=2m_R(E-\epsilon_{\nu l})$. It should be noted that $G^{J}_{\nu Ll}(R)$ is accordingly independent of J.

In the present system, the function $G^{J}_{\nu Ll}(R)$ also contains the information on the hadronic effect caused by the strong interaction between $\bar{p}$ and p. In the present calculation, the hadronic effect is assumed to be negligible for $L \geqslant 1$. Then, $G^{J}_{\nu Ll}(R)$ has the form [11,36]

$$G^{J}_{\nu Ll}(R) = \begin{cases} Q_0[Z_0S_0(R)+C_0(R)] & \text{for} \quad L=0, \\ Q_L S_L(R) & \text{for} \quad L \geqslant 1, \end{cases} \quad (15)$$

where $S_L(R)$ and $C_L(R)$ are the regular and irregular Coulomb functions, respectively; Q_L is the normalization constant; and Z_0 is a complex-valued constant as a result of the $\bar{p}$-p annihilation decay. According to $\kappa^2>0$ or <0, the coefficient Z_0 is expressed in terms of the phase shift η_0 or the quantum defect μ_0 [36,37], i.e.,

$$Z_0 = \begin{cases} \cot\,\eta_0 & \text{for} \quad \kappa^2>0, \\ \cot\,\pi\mu_0 & \text{for} \quad \kappa^2<0. \end{cases} \quad (16)$$

It may be shown that the quantum defect μ_0 extrapolated to $\kappa^2>0$ can be given by [36,37]

$$\cot\,\pi\mu_0 = \cot\,\eta_0\left[1-\exp\left(-\frac{2\pi m_R}{\kappa}\right)\right]^{-1}. \quad (17)$$

The phase shift η_0 is smoothly connected to $\pi\mu_0$.

Because $E_{\mathrm{coll}},\epsilon_{\nu l} \ll 1$ a.u. in the present case, the related $\bar{p}$-p energies are $|\kappa^2/(2m_R)| \sim 0.5$ a.u., and are negligibly small compared to the hadronic scale. Therefore, it is sufficient to obtain the hadronic information in the zero-energy limit. Thus, the coefficient Z_0 (regardless of $\kappa^2 \lesseqgtr 0$) can be accurately expressed in terms of the Coulomb-corrected scattering length Λ [36], i.e.,

$$\cot\,\eta_0 = -\frac{1}{2\pi m_R\Lambda}. \quad (18)$$

The scattering length Λ can be estimated from the hadronic energy shift and width of the $\bar{p}p$ atom in the ground state

by using the Trueman formula [20], and its imaginary part obtained in this way is in good agreement with the value extracted from the low-energy annihilation cross sections in $\bar{p}+p$ hadronic collisions [2,38]. The derivation of the hadronic scattering length using quantum defect theory [37] was also offered [39]. It is of course possible to directly calculate the coefficient Z_0 by using an effective hadronic model potential [2,10,12]. In the present study, the value $\Lambda = (0.88 - 0.64i)$ fm $= (1.7 - 1.2i) \times 10^{-5}$ a.u. presented in Ref. [2] was used.

At the boundary I, the R-matrix $\mathbb{R}^{\mathfrak{d}}_{II}$ including the hadronic effect may be defined by

$$\mathcal{R}^{\mathfrak{d}}_{\nu Ll,\nu' L' l'} = G^J_{\nu Ll}(A)\left[\frac{dG^J_{\nu Ll}}{dR}(A)\right]^{-1}\delta_{\nu\nu'}\delta_{LL'}\delta_{ll'}. \quad (19)$$

In the present case, the Coulomb functions $S_L(R)$ and $C_L(R)$ are insensitive to κ^2 because A is taken to be sufficiently small [37]. Therefore, $\kappa^2 = 0$ can be safely assumed also in the calculation of the R-matrix elements $\mathcal{R}^{\mathfrak{d}}_{\nu Ll,\nu Ll}$, which are thus practically independent of ν and l. For $L \geqslant 1$, since the amplitude of $S_L(R)$ at $R \lesssim A$ is sufficiently small, one can practically set $\mathcal{R}^{\mathfrak{d}}_{\nu Ll,\nu Ll} = 0$. As it turns out, the nonzero R-matrix elements are simply given by

$$\mathcal{R}^{\mathfrak{d}}_{\nu Ll,\nu Ll} = \Omega\,\delta_{L0}, \quad (20)$$

where Ω is a complex-valued constant. Figure 2 shows that Ω is actually independent of κ^2 as long as $|\kappa^2/(2m_R)| \lesssim 10^4$ eV. From the separability of the $\mathbf{R}$ and $\mathbf{r}$ motions in the domain $\mathfrak{d}$, the equalities $\mathbb{R}^{\mathfrak{d}}_{IX} = 0$ and $\mathbb{R}^{\mathfrak{d}}_{XI} = 0$ are satisfied. In a strict sense, the hadronic interaction should be dependent on the nuclear spin [2]. Such effects can be properly taken into account by allowing that Eq. (19) has spin-dependent elements. The annihilation lifetime largely differs for ortho and para e^+e [40], but such difference seems to be small for $\bar{p}p$ [2]. In this study, the spin-averaged value Λ was adopted.

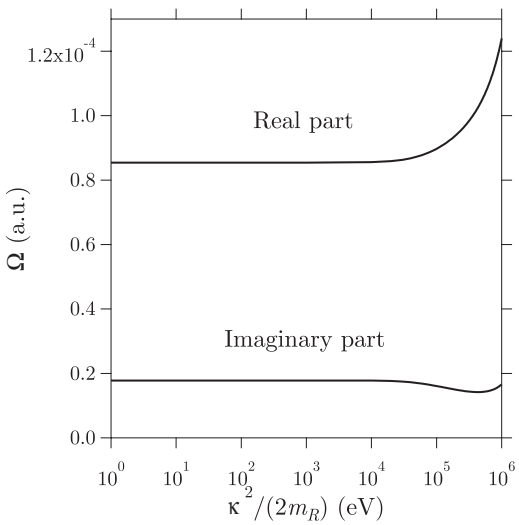

FIG. 2. Hadronic R matrix Ω of $\bar{p}+p$ as a function of the kinetic energy $\kappa^2/(2m_R)$.

C. Domain $\mathfrak{D}$: Three-body Coulomb processes

Around the boundary O_e of the domain $\mathfrak{D}$, one can write the scattering wave function Ψ^{JM} in a form similar to Eq. (7), i.e.,

$$\Psi^{JM}(\mathbf{r},\mathbf{R}) = (Rr)^{-1}\sum_{KLl}\mathcal{Y}^{JM}_{Ll}(\hat{\mathbf{R}},\hat{\mathbf{r}})\Xi_{KL}(R)g^J_{KLl}(r), \quad (21)$$

where a channel function $\Xi_{KL}(R)$ is defined in the range $A \leqslant R \leqslant B$, and is given by [31]

$$\left[-\frac{1}{2m_R}\frac{d^2}{dR^2} + \frac{L(L+1)}{2m_R R^2} - \frac{1}{R} - \frac{\delta(R-A)}{2m_R}\frac{d}{dR} + \frac{\delta(R-B)}{2m_R}\frac{d}{dR} - E_{KL}\right]\Xi_{KL}(R) = 0, \quad (22)$$

with the normalization

$$\int_A^B \Xi_{KL}(R)\Xi_{K'L}(R)dR = \delta_{KK'}. \quad (23)$$

The expansion form of Eq. (21) is useful for obtaining the R matrix at the boundary O_e. For the evaluation of the R matrix at the other boundaries of the domain $\mathfrak{D}$, one can introduce the BO form of Eq. (9) at the boundary $O_{\bar{p}}$ and the expansion form of Eq. (11) at the boundary I.

For numerically calculating the scattering wave function Ψ^{JM} everywhere in the domain $\mathfrak{D}$, it is entirely appropriate to employ the R-matrix basis, which is given by the eigenvalue equation [27–31]

$$(\mathsf{H}+\mathsf{L}-E^J_\rho)\Phi^{JM}_\rho(\mathbf{R},\mathbf{r}) = 0, \quad (24)$$

where

$$\mathsf{L} = -\frac{1}{2m_R A}\delta(R-A)\frac{\partial}{\partial R}R + \frac{1}{2m_R B}\delta(R-B)\frac{\partial}{\partial R}R + \frac{1}{2m_r b}\delta(r-b)\frac{\partial}{\partial r}r \quad (25)$$

is the Bloch operators, and ρ identifies the discrete eigenvalues E^J_ρ. The eigenfunction Φ^{JM}_ρ is normalized to unity for the integration over $\mathfrak{D}$. Using the R-matrix basis Φ^{JM}_ρ, the scattering wave function Ψ^{JM} in the domain $\mathfrak{D}$ can be written as [25]

$$\Psi^{JM}(\mathbf{R},\mathbf{r}) = \sum_\rho \Phi^{JM}_\rho(\mathbf{R},\mathbf{r})\frac{1}{E_\rho - E}\left\langle\Phi^{JM}_\rho\middle|\mathsf{L}\Psi^{JM}\right\rangle_{\mathfrak{D}}, \quad (26)$$

where $\langle\,|\,\rangle_{\mathfrak{D}}$ means the integration over $\mathfrak{D}$.

The channels τ on the boundaries of the domain $\mathfrak{D}$ are given by $\tau = 1\sigma$ for $O_{\bar{p}}$, $\tau = (K,L,l)$ for O_e, and $\tau = (\nu,L,l)$ for I. Substitution of Eqs. (9), (11), or (21) into Eq. (26) provides the relation of the radial functions $F^J_{1\sigma}(R)$, $g^J_{KLl}(r)$, and $G^J_{\nu Ll}(R)$ with their derivatives on each of the boundaries $O_{\bar{p}}$, O_e, and I

in the form [27–31]

$$F^J_{1\sigma}(B) = \mathcal{R}^{\mathfrak{D}}_{1\sigma,1\sigma}\frac{dF^J_{1\sigma}}{dR}(B) + \sum_{K'L'l'}\mathcal{R}^{\mathfrak{D}}_{1\sigma,K'L'l'}\frac{dg^J_{K'L'l'}}{dr}(b) - \sum_{\nu'L'l'}\mathcal{R}^{\mathfrak{D}}_{1\sigma,\nu'L'l'}\frac{dG^J_{\nu'L'l'}}{dR}(A), \quad (27)$$

$$g^J_{KLl}(b) = \mathcal{R}^{\mathfrak{D}}_{KLl,1\sigma}\frac{dF^{Jp}_{1\sigma}}{dR}(B) + \sum_{K'L'l'}\mathcal{R}^{\mathfrak{D}}_{KLl,K'L'l'}\frac{dg^J_{K'L'l'}}{dr}(b) - \sum_{\nu'L'l'}\mathcal{R}^{\mathfrak{D}}_{KLl,\nu'L'l'}\frac{dG^J_{\nu'L'l'}}{dR}(A), \quad (28)$$

$$G^J_{\nu Ll}(A) = \mathcal{R}^{\mathfrak{D}}_{\nu Ll,1\sigma}\frac{dF^{Jp}_{1\sigma}}{dR}(B) + \sum_{K'L'l'}\mathcal{R}^{\mathfrak{D}}_{\nu Ll,K'L'l'}\frac{dg^J_{K'L'l'}}{dr}(b) - \sum_{\nu'L'l'}\mathcal{R}^{\mathfrak{D}}_{\nu Ll,\nu'L'l'}\frac{dG^J_{\nu'L'l'}}{dR}(A), \quad (29)$$

where the elements of the R matrices $\mathbb{R}^{\mathfrak{D}}_{OO},\mathbb{R}^{\mathfrak{D}}_{OI},\mathbb{R}^{\mathfrak{D}}_{IO}$, and $\mathbb{R}^{\mathfrak{D}}_{II}$ with $O = O_{\bar{p}}$ or O_e are defined by

$$\mathcal{R}^{\mathfrak{D}}_{\tau,\tau'} = \frac{1}{2m}\sum_{\rho}\frac{W^J_{\tau,\rho}W^J_{\tau',\rho}}{E_\rho - E}, \quad (30)$$

with

$$W^J_{1\sigma,\rho} = \left\langle (Rr)^{-1}\mathcal{D}^{JM}_{M0}\chi_{1\sigma}\middle|\delta(R-B)\Phi^{JM}_\rho\right\rangle_{\mathfrak{D}}, \quad (31)$$

$$W^J_{KLl,\rho} = \left\langle (Rr)^{-1}\mathcal{Y}^{JM}_{Ll}\Xi_{KL}\middle|\delta(r-b)\Phi^{JM}_\rho\right\rangle_{\mathfrak{D}}, \quad (32)$$

$$W^J_{\nu Ll,\rho} = \left\langle (Rr)^{-1}\mathcal{Y}^{JM}_{Ll}\xi_{\nu l}\middle|\delta(R-A)\Phi^{JM}_\rho\right\rangle_{\mathfrak{D}}. \quad (33)$$

The mass m in Eq. (30) is $m = m_R$ for $\tau' = 1\sigma$ or (ν',L',l') and $m = m_r$ for $\tau' = (K',L',l')$.

The calculation of Eq. (24) is the most laborious part in the present study. For the numerical calculation, the R-matrix eigenfunction $\Phi^{JM}_\rho(\mathbf{R},\mathbf{r})$ in Eq. (24) is expanded as [26,33]

$$\Phi^{JM}_\rho(\mathbf{R},\mathbf{r}) = (Rr)^{-1}\sum_\lambda \mathcal{D}^J_{M\lambda}(\hat{\mathbf{R}})\phi^{J\lambda}_\rho(R,r,\theta). \quad (34)$$

The wave function $\phi^{J\lambda}_\rho(R,r,\theta)$ is numerically solved by using a grid (discrete-variable) representation technique. For the details of this calculation, see Refs. [26,33]. Basically, the grid points were constructed from the zero points of the same orthogonal polynomials as in the $\mu^- + \mathrm{H}$ calculation [26] except for R. The channels of $|\lambda| \leqslant 1$ were included, and the numbers of grid points $(N_r,N_\theta) = (25,4)$ were chosen for (r,θ) associated with the electron motion. Because of the two-boundary problem, the Legendre polynomials are appropriate for R [41,42]. The number of grid points on R is $N_R = 220$ for $J = 0$, $N_R = 210$ for $J = 1$, $N_R = 175$ for $J = 2$, $N_R = 115$ for $J = 3,4$, $N_R = 95$ for $J = 5$–7, and $N_R = 70$ for $J \geqslant 8$. For these choices, sufficient accuracy was achieved: For example, the adiabatic potential $V_{1\sigma}(R)$ was calculated with an error of < 0.05 eV at $R > 1.8$ a.u. and of 0.1–0.2 eV at $R < 1.8$ a.u., and the calculated $1s$ and $30s$ Coulomb energies of $\bar{p}p$ coincide with the accurate values at least to four decimal places in eV. The convergence of the transition probabilities was checked as done in previous studies [26,33], and mostly the error is $< 1\%$. It should be noted that the diagonalization of Eq. (24) is performed by a real-number calculation.

D. Global R matrix for the domain $\mathfrak{d} + \mathfrak{D}$

Next, let us consider the combined domain $\mathfrak{d} + \mathfrak{D}$. Using the local R matrices defined in Secs. II B and II C, the global R matrix $\mathbb{R}^{\mathfrak{d}+\mathfrak{D}}$ on the boundary of the domain $\mathfrak{d} + \mathfrak{D}$ can be given by [27–31]

$$\begin{aligned}
\mathbb{R}^{\mathfrak{d}+\mathfrak{D}}_{OO} &= \mathbb{R}^{\mathfrak{D}}_{OO} - \mathbb{R}^{\mathfrak{D}}_{OI}\left[\mathbb{R}^{\mathfrak{d}}_{II} + \mathbb{R}^{\mathfrak{D}}_{II}\right]^{-1}\mathbb{R}^{\mathfrak{D}}_{IO},\\
\mathbb{R}^{\mathfrak{d}+\mathfrak{D}}_{OX} &= \mathbb{R}^{\mathfrak{D}}_{OI}\left[\mathbb{R}^{\mathfrak{d}}_{II} + \mathbb{R}^{\mathfrak{D}}_{II}\right]^{-1}\mathbb{R}^{\mathfrak{d}}_{IX} = 0,\\
\mathbb{R}^{\mathfrak{d}+\mathfrak{D}}_{XO} &= \mathbb{R}^{\mathfrak{d}}_{XI}\left[\mathbb{R}^{\mathfrak{d}}_{II} + \mathbb{R}^{\mathfrak{D}}_{II}\right]^{-1}\mathbb{R}^{\mathfrak{D}}_{IO} = 0,\\
\mathbb{R}^{\mathfrak{d}+\mathfrak{D}}_{XX} &= \mathbb{R}^{\mathfrak{d}}_{XX} - \mathbb{R}^{\mathfrak{d}}_{XI}\left[\mathbb{R}^{\mathfrak{d}}_{II} + \mathbb{R}^{\mathfrak{D}}_{II}\right]^{-1}\mathbb{R}^{\mathfrak{d}}_{IX} = \mathbb{R}^{\mathfrak{d}}_{XX},
\end{aligned} \quad (35)$$

where $\mathbb{R}^{\mathfrak{d}}_{IX} = 0$ and $\mathbb{R}^{\mathfrak{d}}_{XI} = 0$ have been used. The R matrix $\mathbb{R}^{\mathfrak{d}+\mathfrak{D}}$ has the elements identified by the channels (K,L,l) on the boundary O_e. However, one needs to introduce the global R-matrix elements, which are identified by the scattering channels (N,L,l) on $X + O_e$ and 1σ on $O_{\bar{p}}$ as defined in Sec. II A. This can be achieved by the channel transformation from K to N [31]. Following Ref. [31], the final global R matrix becomes

$$\mathbb{R} = \begin{pmatrix}\mathbb{R}_{\bar{p}\bar{p}} & \mathbb{R}_{\bar{p}e}\\ \mathbb{R}_{e\bar{p}} & \mathbb{R}_{ee}\end{pmatrix} = \mathbb{U}^T\begin{pmatrix}\mathbb{R}^{\mathfrak{d}+\mathfrak{D}}_{O_{\bar{p}}O_{\bar{p}}} & \mathbb{R}^{\mathfrak{d}+\mathfrak{D}}_{O_{\bar{p}}O_e} & 0\\ \mathbb{R}^{\mathfrak{d}+\mathfrak{D}}_{O_eO_{\bar{p}}} & \mathbb{R}^{\mathfrak{d}+\mathfrak{D}}_{O_eO_e} & 0\\ 0 & 0 & \mathbb{R}^{\mathfrak{d}+\mathfrak{D}}_{XX}\end{pmatrix}\mathbb{U}, \quad (36)$$

where "e" (or "$\bar{p}$") stands for $e + \bar{p}p$ (or $\bar{p} + \mathrm{H}$), and the channel transformation matrix $\mathbb{U}$ is

$$\mathbb{U} = \begin{pmatrix}1 & 0\\ 0 & \mathbb{U}_{O_e}\\ 0 & \mathbb{U}_X\end{pmatrix}, \quad (37)$$

with

$$\left(\mathbb{U}_{O_e}\right)_{KLl,NL'l'} = \int_A^B \Xi_{KL}(R)\Upsilon_{NL}(R)dR\,\delta_{LL'}\delta_{ll'} \quad (38)$$

being the overlap between the channel function $\Xi_{KL}(R)$ and the wave function $\Upsilon_{NL}(R)$ of $\bar{p}p$. An explicit form of $\mathbb{U}_X$ is unnecessary in the present calculation for the reason given below.

From Eq. (36), the R matrix $\mathbb{R}^{\mathfrak{d}+\mathfrak{D}}_{XX}$ on the boundary X has a contribution only for $\mathbb{R}_{ee}$ in the way:

$$\mathbb{R}_{ee} = \mathbb{U}^T_{O_e}\mathbb{R}^{\mathfrak{d}+\mathfrak{D}}_{O_eO_e}\mathbb{U}_{O_e} + \mathbb{U}^T_X\mathbb{R}^{\mathfrak{d}+\mathfrak{D}}_{XX}\mathbb{U}_X. \quad (39)$$

At $E_{\mathrm{coll}} \leqslant 0.1$ eV, the capture channels $N \leqslant 30$ are energetically open as seen in Fig. 3, and the emitted electrons have kinetic energies among $E_{\mathrm{H}} - E_{N=30} = 0.273$ and 0.373 eV if the products $\bar{p}p$ are in the $N = 30$ state. (The electron kinetic energies are > 1.247 eV for $N \leqslant 29$.) Igarashi and Gulyás [43] showed that the annihilation effect during the collision of $e + \bar{p}p(N = 30)$ becomes important at electron kinetic energies of $\lesssim 0.05$ eV. This means that the direct annihilation can be neglected in the electron scattering at $r \geqslant b$. (The electron having kinetic energy 0.3 eV runs a distance of about 120 a.u. in a time span of the annihilation

lifetime τ_{30s}.) Then, the relative importance of the second term to the first in the right-hand side of Eq. (39) is roughly estimated by the probability of finding the $\bar{p}$-p distance in the range $R \leqslant A$, i.e., $\int_0^A [\Upsilon_{NL}(R)]^2 dR$. In the present case, this probability is small, $\sim 10^{-3}$, even for the $1s$ state of $\bar{p}p$, and becomes much smaller for $N \gg 1$ or $L \geqslant 1$. Consequently, one can safely neglect the term $\mathbb{U}_X^T \mathbb{R}_{XX}^{\mathfrak{d}+\mathfrak{D}} \mathbb{U}_X$ in Eq. (39).

E. Reaction probabilities and cross sections

The scattering boundary condition in the $e + \bar{p}p$ channel is imposed at a sufficiently large distance $r = r_{\max}$, where the electron radial function $f_{NLl}^J(r)$ in Eq. (7) is represented by the asymptotic form, and the scattering K matrices $\mathbb{K}_{ee}$ and $\mathbb{K}_{e\bar{p}}$ are defined. In the present calculation, the global R matrix given by Eq. (36) was further propagated out to $r_{\max} = 100$ a.u. [41], which is sufficient for the asymptotic analysis at $E_{\rm coll} < E_{N=31} - E_{\rm H} = 0.608$ eV. When $E_{\rm coll} \geqslant 0.608$ eV, the capture channel $N = 31$ becomes additionally open (Fig. 3). If the collision energy is just above this threshold, very slow electrons can be emitted, and accordingly $r_{\max}$ must be taken much larger. Furthermore, for such slow-electron emission, the direct annihilation during the collision would be non-negligible.

At $E_{\rm coll} \leqslant 0.1$ eV, one can neglect the partial waves of $J \geqslant 18$, for which the classical outer turning point in the R motion is > 5 a.u. (cf. Fig. 3). The radial function $F_{1\sigma}^J(R)$ in Eq. (9) at $R = B$ can be expressed as

$$F_{1\sigma}^J(B) = \mathfrak{S}_{1\sigma}^J(B)\delta_{1\sigma,\alpha_0} + \mathfrak{C}_{1\sigma}^J(B)\mathcal{K}_{1\sigma,\alpha_0}^J, \tag{40}$$

where $\mathcal{K}_{1\sigma,\alpha_0}^J$ are the elements of the scattering K matrix $\mathbb{K}_{\bar{p}\bar{p}}$ or $\mathbb{K}_{\bar{p}e}$, α_0 represents the initial channel, and $\mathfrak{S}_{1\sigma}^J(R)$ and

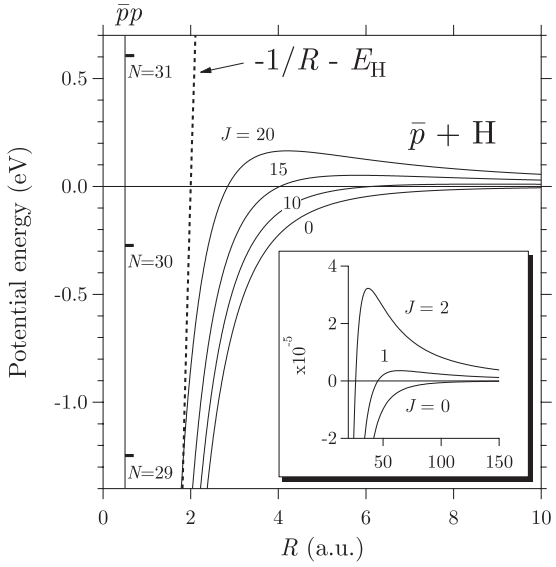

FIG. 3. Effective potential of the $\bar{p} + \mathrm{H}$ system (the sum of the centrifugal and 1σ BO potentials) as a function of the relative distance R for the total angular momentum quantum numbers $J = 0, 1, 2, 10, 15$, and 20. Also shown is the potential curve of the $\bar{p} + p$ system, i.e., $-1/R - E_{\rm H}$. The $\bar{p}p$ energy levels E_N are indicated on the left side. The energies are measured from the ground-state energy $E_{\rm H}$ of H.

$\mathfrak{C}_{1\sigma}^J(R)$ are the reference functions for the adiabatic potential $V_{1\sigma}(R)$, having the asymptotic forms:

$$\begin{aligned} \mathfrak{S}_{1\sigma}^J(R) &\to \left(\frac{m_R}{2\pi k}\right)^{1/2} \sin(kR - J\pi/2), \\ \mathfrak{C}_{1\sigma}^J(R) &\to \left(\frac{m_R}{2\pi k}\right)^{1/2} \cos(kR - J\pi/2), \end{aligned} \tag{41}$$

with $k^2 = 2m_R E_{\rm coll}$. For $E_{\rm coll} \geqslant 10^{-5}$ eV, the values $\mathfrak{S}_{1\sigma}^J(B)$ and $\mathfrak{C}_{1\sigma}^J(B)$ at $R = B$ are obtained by the backward propagation of the WKB solutions at $R = 150$ a.u. For lower energies, the starting values are given by the spherical Bessel and Neumann functions at $R = 500$ or 1000 a.u. The BO potential at $R > 15$ a.u. is replaced by the asymptotic polarization potential $V_{\rm pol}(R) = -\alpha_{\rm pol}/(2R^4)$, with $\alpha_{\rm pol}$ being the polarizability of H. The difference between $V_{1\sigma}(R)$ and $V_{\rm pol}(R)$ is 0.476% at $R = 15$ a.u..

The K matrix $\mathbb{K}$ is calculated directly from the global R matrix $\mathbb{R}$, as described in Ref. [25]. From the K matrix, one can obtain the scattering S matrix $\mathbb{S}$ in a usual manner. Then, the probability of the capture into the (N,L,l) product channel is given by

$$P_{\rm cap}^J(N,L,l) = \left|\mathcal{S}_{NLl,1\sigma}^J\right|^2, \tag{42}$$

where $\mathcal{S}_{NLl,1\sigma}^J$ are the scattering S-matrix elements for the capture reaction. We define the total capture probability summed over all the final channels by

$$P_{\rm cap}^J = \sum_{NLl} P_{\rm cap}^J(N,L,l), \tag{43}$$

and the product-state selected capture probabilities by

$$P_{\rm cap}^J(N,L) = \sum_{l} P_{\rm cap}^J(N,L,l), \tag{44}$$

$$P_{\rm cap}^J(N) = \sum_{Ll} P_{\rm cap}^J(N,L,l), \tag{45}$$

$$P_{\rm cap}^J(L) = \sum_{Nl} P_{\rm cap}^J(N,L,l). \tag{46}$$

Since the hadronic R matrix $\mathbb{R}_{II}^{\mathfrak{d}}$ is complex valued, the K matrix cannot be taken real valued, and hence the S matrix does not satisfy the unitarity. The loss of the probability can be considered as being due to the annihilation decay. Therefore, the probability of the direct annihilation during the collision can be defined by the probability loss

$$P_{\rm ann}^J = 1 - P_{\rm cap}^J - \left|\mathcal{S}_{1\sigma,1\sigma}^J\right|^2, \tag{47}$$

where $\mathcal{S}_{1\sigma,1\sigma}^J$ is the S-matrix element for the elastic collision.

The total capture cross section is

$$\sigma_{\rm cap} = \frac{\pi}{k^2} \sum_J (2J+1) P_{\rm cap}^J. \tag{48}$$

In the same way, one can define the direct annihilation cross section $\sigma_{\rm ann}$ and the product-state selected capture cross sections $\sigma_{\rm cap}(N,L)$, $\sigma_{\rm cap}(N)$, and $\sigma_{\rm cap}(L)$.

III. RESULTS

A. Two-body $\bar{p} + p$ system

First, let us consider the 2B collisions of $\bar{p} + p$ as a simple case. From Eq. (15), the S matrix for the s wave is given by

$$\mathbb{S}^0_{\bar{p}+p} = \frac{Z_0 + i}{Z_0 - i}. \tag{49}$$

The probability of annihilation in $\bar{p} + p$ can be defined by

$$P^0_{\bar{p}+p} = 1 - \left|\mathbb{S}^0_{\bar{p}+p}\right|^2. \tag{50}$$

In the zero-energy limit [Eq. (18)], the probability becomes $P^0_{\bar{p}+p} = 0.240$. For the p wave, the classical turning point in the R motion at $\kappa^2 \simeq 0$ is $\sim 10^{-3}$ a.u., which is much larger than R_0. As is to be expected, only the s wave contributes to the annihilation in the $\bar{p} + p$ collisions in the present energy range.

Next, let us test the present R-matrix method for the energy level of the $\bar{p}p$ atom including the hadronic effect. The continuity of the R matrix at $R = A$ means $\mathbb{R}^{\mathfrak{d}}_{II} = -\mathbb{R}^{\mathfrak{D}}_{II}$ (the electronic degrees of freedom are excluded). The hadronic R matrix $\mathbb{R}^{\mathfrak{d}}_{II}$ is identical to the one given by Eq. (19) or (20). In the 2B system of $\bar{p} + p$, $\mathbb{R}^{\mathfrak{D}}_{II}$ can be expressed in terms of only $\Xi_{KL}(A)$ and E_{KL} in a form similar to Eq. (30). Explicitly, $\mathbb{R}^{\mathfrak{d}}_{II} = -\mathbb{R}^{\mathfrak{D}}_{II}$ provides for $L = 0$,

$$\Omega = -\frac{1}{2m_R} \sum_K \frac{[\Xi_{KL=0}(A)]^2}{E_{KL=0} - E_{\bar{p}p}}. \tag{51}$$

If B is taken sufficiently large, and the energy dependence of Ω is properly taken into account, the solution $E_{\bar{p}p}$ in Eq. (51) represents the bound-state energy of $\bar{p}p$. In the case that Ω is complex valued, the energy level is expressed in the form $E_{\bar{p}p} = E_N + \Delta E_{NL} - i\Gamma_{NL}/2$. Applying first-order perturbation theory to Eq. (51), one can show for the energy-level shift and the width

$$\begin{aligned} \Delta E_{NL=0} &= -\left[2m_R \mathrm{Re}\,\Omega + \Theta^{(1)}_{NL=0}\right]/\Theta^{(2)}_{NL=0}, \\ \Gamma_{NL=0} &= 4m_R \mathrm{Im}\,\Omega/\Theta^{(2)}_{NL=0}, \end{aligned} \tag{52}$$

with

$$\Theta^{(1)}_{NL} = \sum_K \frac{[\Xi_{KL}(A)]^2}{E_{KL} - E_N}, \quad \Theta^{(2)}_{NL} = \sum_K \frac{[\Xi_{KL}(A)]^2}{(E_{KL} - E_N)^2}. \tag{53}$$

Using the complex-valued Ω given in Sec. II B (and hence assuming that Ω is independent of energy), Eq. (52) provides $\Delta E_{1s} = 778$ eV and $\Gamma_{1s} = 1120$ eV, while the x-ray measurements indicate $\Delta E_{1s} = 730$ eV and $\Gamma_{1s} = 1060$ eV [2].

In the special case that $\bar{p}$ and p are point charges, Eq. (15) becomes $G^J_{\nu LI}(R) = Q_L S_L(R)$ for all L, and Ω in Eqs. (19) and (20) is simply given by

$$\Omega = \Omega_{\mathrm{PC}} \equiv S_{L=0}(A)\left[\frac{dS_{L=0}}{dR}(A)\right]^{-1}, \tag{54}$$

which is a real number. In this case, solving Eq. (51) should provide the hydrogenic energy level $E_{\bar{p}p} = E_N$. Let us assume that Ω_{PC} can always be evaluated at the fixed energy $\kappa^2 = 0$. Then, one can obtain from Eq. (51) the lowest hydrogenic energy $E_{\bar{p}p} = -459.453$ a.u., while the accurate hydrogenic $1s$ energy is $E_{N=1} = -459.038$ a.u. If the energy dependence of Ω_{PC} is properly taken into account in Eq. (51), an accurate numerical result can definitely be obtained. In the present study of $\bar{p} + \mathrm{H}$, very high states of $N \sim 30$ participate (namely, $E_{N=30} \sim 0$ as compared to $E_{N=1}$), and thereby the error due to the use of $\Omega = \Omega_{\kappa^2=0}$ is estimated to be much less than 0.1%.

TABLE I. Barrier heights E^J_{eff} of the effective potential.

J	E^J_{eff} (eV)	J	E^J_{eff} (eV)	J	E^J_{eff} (eV)
1	3.58×10^{-6}	7	2.78×10^{-3}	13	2.94×10^{-2}
2	3.23×10^{-5}	8	4.59×10^{-3}	14	3.93×10^{-2}
3	1.29×10^{-4}	9	7.17×10^{-3}	15	5.16×10^{-2}
4	3.59×10^{-4}	10	1.07×10^{-2}	16	6.66×10^{-2}
5	8.07×10^{-4}	11	1.54×10^{-2}	17	8.49×10^{-2}
6	1.57×10^{-3}	12	2.16×10^{-2}	18	1.07×10^{-1}

B. Annihilation and capture probabilities

As seen in Fig. 3, the effective potential of $\bar{p} + \mathrm{H}$ has a barrier for $\bar{p}$ approaching H from infinity except for $J = 0$. Let E^J_{eff} be the height of the effective potential barrier. The values of E^J_{eff} for $J = 1$–18 are listed in Table I. The condition $E_{\mathrm{coll}} < E^J_{\mathrm{eff}}$ means that the motion of $\bar{p}$ coming very close to H is classically forbidden. Therefore, if $E_{\mathrm{coll}} \ll E^J_{\mathrm{eff}}$, no reactions are expected to take place for the partial wave J.

Figure 4 shows the direct annihilation probability P^J_{ann} defined by Eq. (47) at low collision energies $E_{\mathrm{coll}} = 10^{-8}$–$10^{-4}$ eV. As stated before, this "annihilation" means the decay event occurring during the collision. At very low energies $E_{\mathrm{coll}} < 10^{-6}$ eV, only the $J = 0$ wave predominantly contributes to the annihilation. The probability P^J_{ann} for $J = 0$ is proportional to $(E_{\mathrm{coll}})^{1/2}$ at $E_{\mathrm{coll}} \lesssim 10^{-7}$ eV as expected generally in the low-energy limit of exothermic reaction [44,45], and becomes nearly constant at high energies $E_{\mathrm{coll}} > 10^{-5}$ eV.

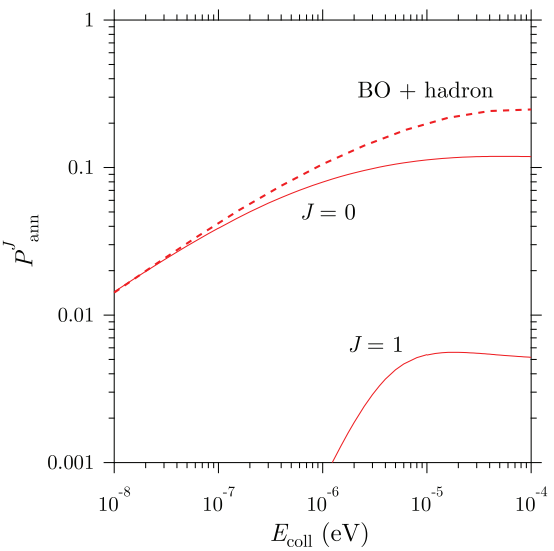

FIG. 4. (Color online) Direct annihilation probabilities P^J_{ann} at collision energies $E_{\mathrm{coll}} = 10^{-8}$–$10^{-4}$ eV. "BO + hadron" is the direct annihilation probability for $J = 0$ obtained by using the BO potential $V_{1\sigma}(R)$ and the hadronic boundary condition of Eq. (19) at $R = A$.

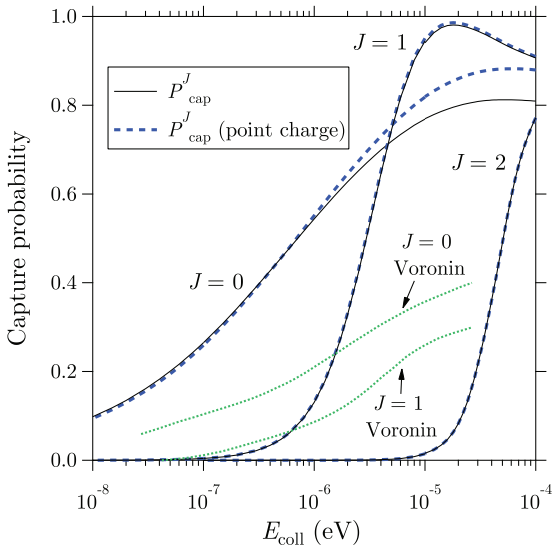

FIG. 5. (Color online) Capture probabilities $P^J_{\rm cap}$ at collision energies $E_{\rm coll} = 10^{-8}$–10^{-4} eV. "$P^J_{\rm cap}$ (point charge)" is the capture probability obtained by using the point-charge approximation ($\Omega = \Omega_{\rm PC}$). The results of Voronin and Carbonell [10] are also shown.

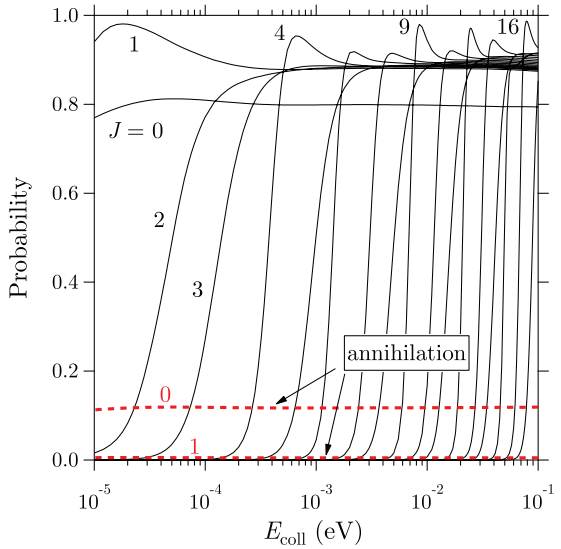

FIG. 6. (Color online) Capture and direct annihilation probabilities $P^J_{\rm cap}$ and $P^J_{\rm ann}$ at collision energies $E_{\rm coll} = 10^{-5}$–10^{-1} eV.

The probability $P^J_{\rm ann}$ for $J = 1$ grows at $E_{\rm coll} \gtrsim 10^{-6}$ eV, but its ratio to $P^{J=0}_{\rm ann}$ remains very small ($P^{J=1}_{\rm ann}/P^{J=0}_{\rm ann} < 0.05$). In a good approximation, the annihilation is always negligible for $J \geqslant 1$. For comparison, also shown are the direct annihilation probabilities for $J = 0$ calculated by using a BO model: The BO potential $V_{1\sigma}(R)$ is assumed to be $-1/R - E_{\rm H}$ at $R \leqslant R_{\rm FT}$, and the problem is solved simply as a potential scattering by $V_{1\sigma}(R)$ with the hadronic boundary condition of Eq. (19) at $R = A$. In the BO model, the radial wave function has a complex-valued phase shift, and hence the annihilation probability can be evaluated. The BO potential was used for the calculation of the hadronic annihilation in the systems of $\mathrm{H} + \bar{\mathrm{H}}$ [9,11] and $\mathrm{He} + \bar{\mathrm{H}}$ [46]. In the present case, the BO model is highly satisfactory at very low energies ($E_{\rm coll} < 10^{-7}$ eV), but provides about twice as large as the accurate value at high energies where the BO annihilation probability becomes just equal to the 2B probability $P^0_{\bar{p}+p}$ because of $V_{1\sigma}(R) = -1/R - E_{\rm H}$ at $R \leqslant R_{\rm FT}$ (see also Ref. [9]).

The capture probability $P^J_{\rm cap}$ in the same energy range as that of Fig. 4 is shown in Fig. 5. At $E_{\rm coll} < 10^{-7}$ eV, the contribution of $J \geqslant 1$ to the capture is negligible, and the probability $P^{J=0}_{\rm cap}$ as well as $P^{J=0}_{\rm ann}$ is proportional to $(E_{\rm coll})^{1/2}$. The capture probabilities for $J = 0$ and 1 at very low energies were calculated by Voronin and Carbonell [10]. Their results are also presented in Fig. 5, and are too small compared with the present ones except for the $J = 1$ wave at very low energies.

The calculation was also made for the capture probabilities by assuming that $\bar{p}$ and p are point charges (and hence the $\bar{p}p$ atom is purely hydrogenic). This point-charge approximation was achieved by using $\Omega_{\rm PC}$ [Eq. (54)] for Ω in Eq. (20). It can be found that the point-charge approximation is always good for $J \geqslant 1$. This is in accordance with the fact that $P^J_{\rm ann}$ is indeed very small for $J \geqslant 1$. In the case of $J = 0$, although the point-charge approximation overestimates $P^{J=0}_{\rm cap}$ at high energies, it works satisfactorily at low energies $E_{\rm coll} \lesssim 10^{-6}$ eV: "$P^{J=0}_{\rm cap}$ (point charge)"$/P^{J=0}_{\rm cap} = 0.96$–$0.98$ at $E_{\rm coll} \leqslant 10^{-7}$ eV. This may seem to be surprising since the collision time gets much longer with further decreasing energy. At very low energies, however, one should notice that all the reaction probabilities ($P^{J=0}_{\rm ann}$ and $P^{J=0}_{\rm cap}$) become small since the interaction at small distances is less important. In such a case, it is expected that the coupling between the hadronic and atomic channels becomes weak as well [44]. Thus, one can expect the applicability of the point-charge approximation for the capture at very low energies. Also for the same reason, the direct annihilation probability at very low energies can be explained adequately by the simple BO model as seen in Fig. 4. At energies where the capture probability is significantly large, the relative motion of $\bar{p} + \mathrm{H}$ is dominated by the reaction dynamics of the capture. When $E_{\rm coll} \gtrsim 10^{-6}$ eV, accordingly the BO model, which disregards the details of the capture dynamics, fails to produce an accurate annihilation probability.

The direct annihilation and capture probabilities at high collision energies $E_{\rm coll} = 10^{-5}$–10^{-1} eV are shown together in Fig. 6. The capture probabilities were calculated for all the partial waves up to $J = 17$. The annihilation probability is almost constant ($P^{J=0}_{\rm ann} = 0.113$–$0.119$) in the energy range of $E_{\rm coll} = 10^{-4}$–10^{-1} eV. The capture probabilities are also nearly constant at $E_{\rm coll} \gtrsim E^J_{\rm eff}$: The constant values are close to unity ($\sim$0.9) except for the $J = 0$ wave which is largely affected by the annihilation channel ($P^{J=0}_{\rm cap} = 0.810 - 0.794$ at $E_{\rm coll} = 10^{-3}$–10^{-1} eV). It is realized that the present system is highly active for the reaction channels. If the radial motion between $\bar{p}$ and H were treated classically, the capture probabilities would have the form of a step function with the argument $E_{\rm coll} - E^J_{\rm eff}$ [26]. Actually, penetration or reflection occurs around the barrier of the effective potential, and the probability exhibits a smooth variation with $E_{\rm coll}$ in the vicinity of $E_{\rm coll} = E^J_{\rm eff}$. In the present system, no potential (shape) resonances are present at $E_{\rm coll} < E^J_{\rm eff}$. The Bohr-Sommerfeld quantization condition shows that the BO potential $V_{1\sigma}(R)$ can support a single quasibound state for several partial waves in the energy range $0 < E_{\rm coll} < E^J_{\rm eff}$. However, provided that the system has a high reactivity such as in the present case, it

seems that a quasistationary wave cannot be maintained inside the potential barrier [47].

For the partial waves of $J = 1$, 4, 6, 7, 9, 10, 12, 13, 15, and 16, the capture probability shows a clear peaklike structure at collision energies just above $E^J_{\rm eff}$. A similar structure was also found in the $\mu^- + {\rm H}$ system [26]. Though this structure is not found in a classical treatment and is seemingly a resonance, the analysis using the scattering time-delay matrix [48] indicates that the peak cannot be attributed to an unequivocal resonance phenomena, as the same conclusion was also arrived at for $\mu^- + {\rm H}$ [26]. In Ref. [47], the capture probabilities in $\bar{p} + {\rm H}$ were calculated by using a local complex potential model at $E_{\rm coll} \geqslant 10^{-2}$ eV, and a peaklike structure just above $E^J_{\rm eff}$ was generated for the same partial waves ($J \geqslant 10$) other than $J = 15$. It is evident that the barrier top of the effective potential is responsible for the peaklike structure. In the case of a simple rectangular potential barrier, interference between an incoming wave and an over-barrier reflected wave can cause an oscillatory structure in the transmission probability at energies above the barrier [49]. However, a uniform semiclassical method, using the mapping of the potential barrier to a parabolic potential, shows that the transmission probability becomes a monotonic function of energy [50,51]. Very recently, Gao [52] investigated the quantal version of the Langevin model [53], and found no peaklike structure in the transmission probability for the $-1/R^4$ form of potential. The quantal Langevin model is realized by the assumption that no reflection occurs by any other short-range interactions. In the present system, the non-negligible deviation of the total reaction probability from unity ($P^J_{\rm cap} + P^J_{\rm ann} \sim 0.9$) far above the barrier suggests that the assumption of no reflection would not be fully accepted. As will be shown elsewhere, the interference with an outgoing wave induced by short-range interactions is considered to be the cause of the present peaklike structure, and it may be identified as a kind of resonance.

C. Product-state distribution in the capture

Figure 7 shows the L-state selected capture cross section multiplied by the collision energy, $E_{\rm coll} \times \sigma_{\rm cap}(L)$, plotted as a function of $E_{\rm coll}$. In the present energy range, since the open capture channels are $N \leqslant N_{\rm max} = 30$, all the angular momentum states up to $L_{\rm max} = N_{\rm max} - 1 = 29$ can be produced in principle. However, it is seen that only low states limited to $L \leqslant L_{\rm upper} \ll L_{\rm max}$ are allowed at each $E_{\rm coll}$, and the upper limit $L_{\rm upper}$ increases with $E_{\rm coll}$. Since a slow emitted electron can carry away only a low angular momentum $l \sim 0$, the major capture channel in the specified partial wave J is $L \simeq J$. Considering that the barrier height $E^J_{\rm eff}$ increases with J (Fig. 3), one can define a certain total angular momentum $J_{\rm max}$ such that $E_{\rm coll} > E^J_{\rm eff}$ only if $J \leqslant J_{\rm max}$. Thus, it is expected that $L_{\rm upper} \simeq J_{\rm max}$. It should be mentioned that the situation is quite different from that of the capture at much higher collision energies [5,24,54]. If the BO potential $V_{1\sigma}(R)$ is approximated by the asymptotic polarization form $V_{\rm pol}(R)$ in the barrier region, $J_{\rm max}$ can be given by the orbiting angular momentum $J_{\rm orb} = (8\alpha_{\rm pol} m_R^2 E_{\rm coll})^{1/4}$. One can find that $J_{\rm orb}$ is mostly a good estimate of $L_{\rm upper}$.

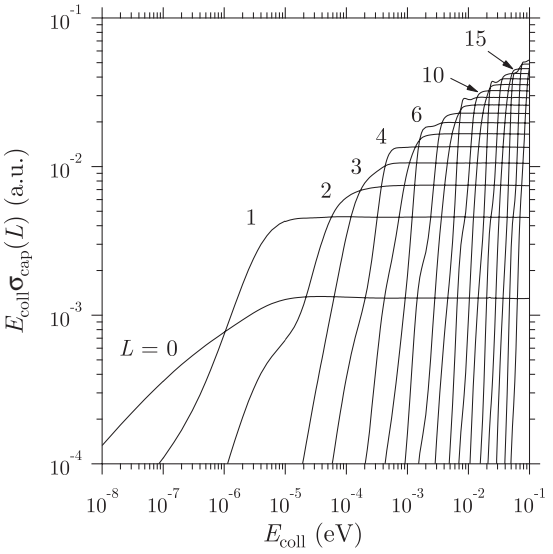

FIG. 7. $E_{\rm coll}$ times L-state selected capture cross sections $E_{\rm coll} \times \sigma_{\rm cap}(L)$ at collision energies $E_{\rm coll} = 10^{-8}$–10^{-1} eV.

Figure 7 shows that $E_{\rm coll}\sigma_{\rm cap}(L)$ becomes nearly constant at high energies. This is because the contribution to the capture cross section $\sigma_{\rm cap}(L)$ mainly comes from the partial wave $J \simeq L$ and the capture probability $P^J_{\rm cap}$ is almost constant at $E_{\rm coll} \gtrsim E^J_{\rm eff}$ (Fig. 6). Thus, the L-selected capture cross section $\sigma(L)$ has the energy dependence $(E_{\rm coll})^{-1}$ when it has a prominent value.

Figure 8 shows the N-state selected capture cross section multiplied by the square root of the collision energy, $(E_{\rm coll})^{1/2} \times \sigma(N)$, which has the same energy dependence as the rate constant. Except for some undulations, $(E_{\rm coll})^{1/2}\sigma(N)$ seems to undergo only a slight change with energy on the whole. Therefore, the N-selected capture cross section $\sigma(N)$ has entirely the energy dependence $(E_{\rm coll})^{-1/2}$. The undulation appears particularly as a result of gathering the peaklike structures present in some capture probabilities $P^J_{\rm cap}$ at $E_{\rm coll} \sim E^J_{\rm eff}$:

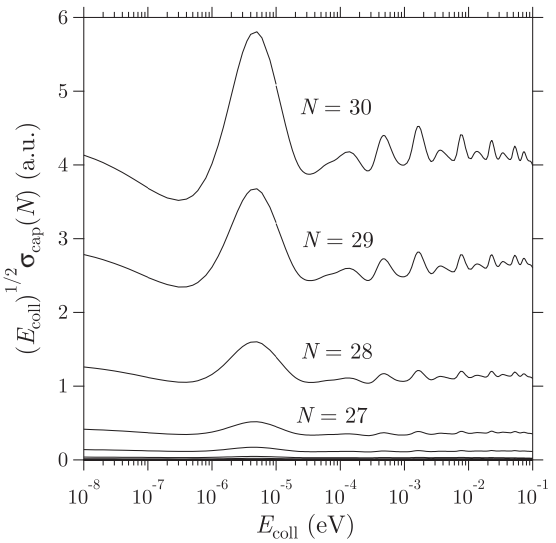

FIG. 8. $(E_{\rm coll})^{1/2}$ times N-state selected capture cross sections $(E_{\rm coll})^{1/2} \times \sigma_{\rm cap}(N)$ at collision energies $E_{\rm coll} = 10^{-8}$–10^{-1} eV.

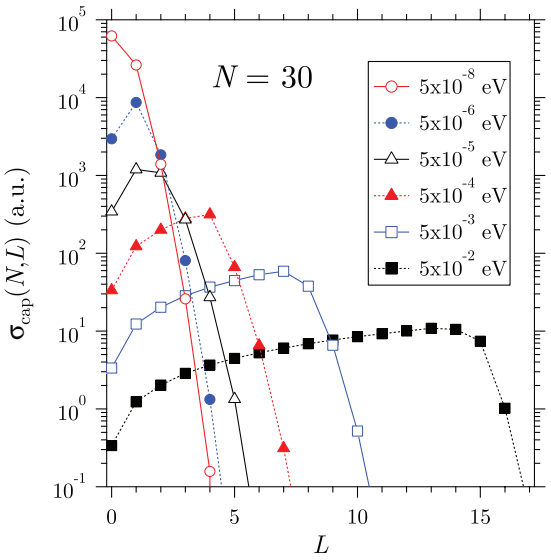

FIG. 9. (Color online) (N,L)-state selected capture cross sections $\sigma(N,L)$ for $N = 30$ as a function of the angular momentum quantum number L at several collision energies E_{coll}.

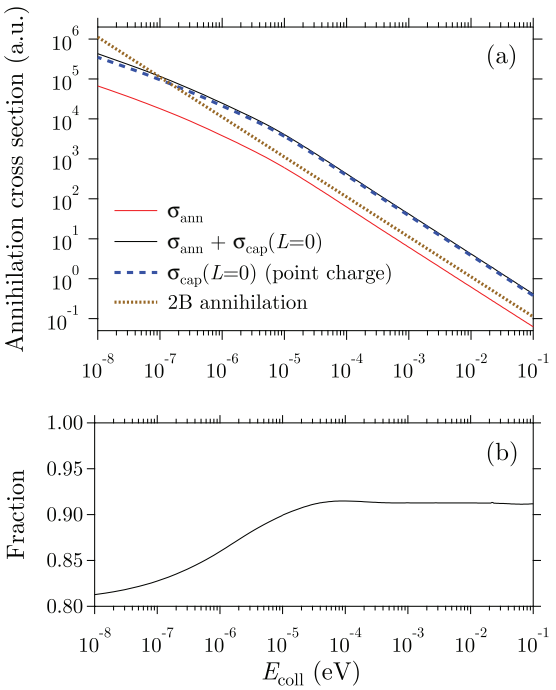

FIG. 10. (Color online) (a) Direct annihilation cross sections σ_{ann} at collision energies $E_{coll} = 10^{-8}$–10^{-1} eV. Also shown are the total annihilation cross section $\sigma_{ann}^{tot} = \sigma_{ann} + \sigma_{cap}(L=0)$, the capture cross section "$\sigma_{cap}(L=0)$ (point charge)" obtained by using the point-charge approximation, and the 2B annihilation cross section σ_{ann}^{2B} of $\bar{p} + p$. (b) The fraction "$\sigma_{cap}(L=0)$ (point charge)"$/\sigma_{ann}^{tot}$ at collision energies $E_{coll} = 10^{-8}$–10^{-1} eV.

For example, the largest peak at $E_{coll} \sim 5 \times 10^{-6}$ eV originates in the $J = 1$ partial wave. In the quantal Langevin model, the transmission probability versus energy is nearly a step function, and this also generates an undulation structure in the transmission rate constant [52]. In the present system, the undulation is much more enhanced than that expected in the Langevin model owing to the occurrence of the peaklike structure.

The cross section $\sigma_{cap}(N)$ at the same energy becomes the largest always for $N = N_{max}(=30)$, which is the highest open capture channel. The capture into very low N states, in the case of which the emitted electrons must have huge kinetic energies, is only rarely realized. Voronin and Carbonell [10] obtained a somewhat different result that the most populated state ($N = N_0$) is 29 rather than 30 at $E_{coll} < 2.72 \times 10^{-7}$ eV. Tong *et al.* [24] calculated the capture cross sections $\sigma_{cap}(N)$ for $\bar{p} + \text{H}$ at energies $E_{coll} \geqslant 2.72$ eV, and found that the most populated state is $N_0 = N_{max}(=33)$ at $E_{coll} = 2.72$ eV and becomes $N_0 < N_{max}$ at $E_{coll} \geqslant 5.44$ eV. The results except for Voronin and Carbonell [10] indicate that the low-energy capture leads to preferably slower-electron emission.

Figure 9 shows the L-state distribution of the capture products $\bar{p}p$ in the $N = N_{max}(=30)$ state for several collision energies. The L distribution becomes broader as the energy increases, and has the maximum at $L \simeq J_{orb}$. In the present energy range, so-called circular orbits of $\bar{p}p$ ($L \simeq N - 1$), which are the most stable against annihilation within the same N, can hardly be formed in the capture. The efficient formation of the circular orbits requires much higher collision energies [5,24,54]. The distribution of low L states reflects the statistical weight, i.e., $\sigma(N,L) \propto (2L + 1)$, until L reaches $\sim J_{orb}$.

D. Annihilation and capture cross sections

Figure 10 shows the direct annihilation cross sections σ_{ann} at collision energies $E_{coll} = 10^{-8}$–10^{-1} eV. In the present study, the $\bar{p}p$ atoms in the s states annihilate as time passes (indirect annihilation). Accordingly, one may define the total (direct plus indirect) annihilation cross section by

$$\sigma_{ann}^{tot} = \sigma_{ann} + \sigma_{cap}(L = 0). \tag{55}$$

This total cross section is compared with $\sigma_{cap}(L = 0)$ obtained by using the point-charge approximation. (By definition, $\sigma_{ann} = 0$ in the point-charge approximation.) Figure 10 includes these two cross sections and also the fraction "$\sigma_{cap}(L = 0)$ (point charge)"$/\sigma_{ann}^{tot}$ to clarify their difference. About 90% of the total annihilation cross section σ_{ann}^{tot} can be reproduced by the point-charge approximation if $E_{coll} \gtrsim 10^{-5}$ eV. At low energies $E_{coll} < 10^{-5}$ eV, the difference becomes larger although the capture probability $P_{cap}^{J=0}$ can be estimated adequately by the point-charge approximation (Fig. 5).

For comparison, the annihilation cross section $\sigma_{ann}^{2B} = \pi k^{-2} P_{\bar{p}+p}^{0}$ in the 2B $\bar{p} + p$ collisions, with the use of $P_{\bar{p}+p}^{0} = 0.240$ in the zero-energy limit, is also plotted in Fig. 10. The 2B annihilation cross section σ_{ann}^{2B} is larger than σ_{ann} at all the energies, but smaller than σ_{ann}^{tot} at $E_{coll} > 10^{-7}$ eV. Thus, the neutral target is found to play an important role not only for the capture of $\bar{p}$ but also for the annihilation of $\bar{p}$. Because of the Coulomb attraction between $\bar{p}$ and p, the 2B cross section σ_{ann}^{2B} has the energy dependence $(E_{coll})^{-1}$ even at $E_{coll} \to 0$, and becomes larger than σ_{ann}^{tot} at very low energies $E_{coll} < 10^{-7}$ eV. If $E_{coll} > 10^{-5}$ eV, since the direct annihilation and capture probabilities for $J = 0$ are almost independent of E_{coll}, the cross sections σ_{ann} and σ_{ann}^{tot} have the same energy dependence $(E_{coll})^{-1}$ as that of σ_{ann}^{2B}. At very low energies, however, σ_{ann} and σ_{ann}^{tot} have the $(E_{coll})^{-1/2}$ energy dependence.

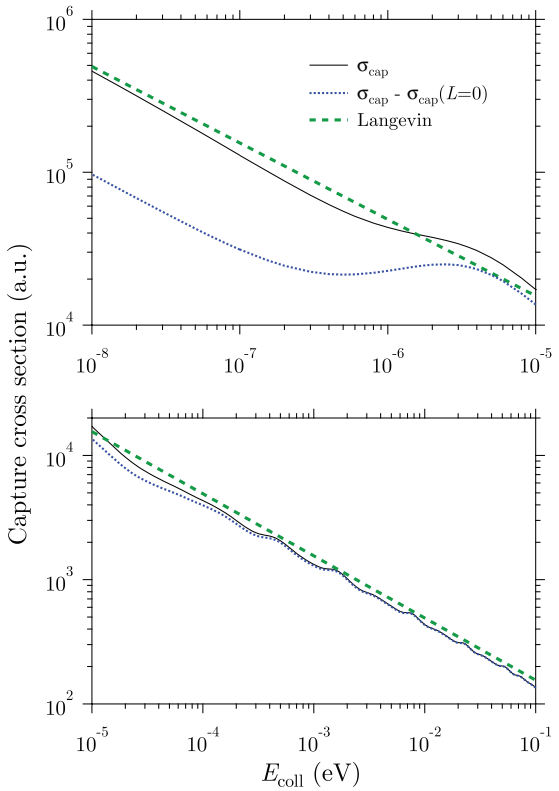

FIG. 11. (Color online) Capture cross sections $\sigma_{\rm cap}$ at collision energies $E_{\rm coll} = 10^{-8}$–10^{-1} eV. Also shown are $\sigma_{\rm cap}^{\rm net} = \sigma_{\rm cap} - \sigma_{\rm cap}(L = 0)$ and the classical Langevin cross section $\sigma_{\rm Langevin}$.

Figure 11 shows the total capture cross section $\sigma_{\rm cap}$ at collision energies $E_{\rm coll} = 10^{-8}$–10^{-1} eV. The structure of undulation seen in the cross section is a real one. When $E_{\rm coll} \lesssim 10^{-7}$ eV, this undulation becomes absent since the partial waves $J \geqslant 1$ are negligible. As exemplification of a typical low-energy ion-molecule reaction, also plotted in Fig. 11 is the classical Langevin (orbiting) cross section $\sigma_{\rm Langevin} = \pi(2\alpha_{\rm pol}/E_{\rm coll})^{1/2}$ [53]. The capture cross section has, on average, roughly the same energy dependence as $\sigma_{\rm Langevin}$, and is even close to $\sigma_{\rm Langevin}$ at very low energies. The latter is rather accidental: The classical picture should be poor at very low energies, where only $J = 0$ can contribute to the capture and the quantal Langevin cross section becomes indeed much larger than $\sigma_{\rm Langevin}$ [52]. As discussed just before, the production of the s states may be finally excluded as the capture process. Then, one may define the net capture cross section given by

$$\sigma_{\rm cap}^{\rm net} = \sigma_{\rm cap} - \sigma_{\rm cap}(L = 0). \tag{56}$$

It is seen in Fig. 11 that the difference between $\sigma_{\rm cap}^{\rm net}$ and $\sigma_{\rm cap}$ becomes prominent at $E_{\rm coll} < 10^{-4}$ eV. The net capture cross section $\sigma_{\rm cap}^{\rm net}$ does not tend to zero at $E_{\rm coll} \to 0$ since the $J = 0$ wave can produce a non-negligible amount of $\bar{p}p$ in the p or d states.

IV. SUMMARY AND DISCUSSION

A unified quantum-mechanical treatment of $\bar{p}$-p annihilation and $\bar{p}p$ formation in $\bar{p}$ + H collisions has been developed by using an R-matrix method. The annihilation decay has been expressed as complex-valued R-matrix elements on the inner boundary set at a very small $\bar{p}$-p distance $R = A$ ($=10^{-4}$ a.u.). This hadronic R matrix, which is actually independent of energy, can be deduced from energy-level shifts and widths obtained by x-ray measurements of $\bar{p}p$ or from scattering lengths obtained by collision experiments of $\bar{p} + p$. The R-matrix diagonalization problem of the Coulomb 3B ($\bar{p}$-p-e) dynamics has been solved only in a purely atomic domain defined by $R \in (A, B)$ and $r \in (0, b)$, with $B = 2.7$ a.u. and $b = 8$ a.u. Although the hadronic R-matrix elements are complex numbers, the R-matrix diagonalization in the atomic domain can be made by a real-number calculation.

Propagating the R matrix to an appropriate outer boundary, one has been able to calculate the probabilities of the annihilation and the $\bar{p}$ capture. In the calculation of the asymptotic $e + \bar{p}p$ scattering, the annihilation effect of $\bar{p}p$ has been neglected at $E_{\rm coll} < E_{N=31} - E_{\rm H}$ since the time scale of electron emission is shorter than the annihilation lifetime. However, if the collision energy is just above the threshold $E_N - E_{\rm H}$ ($N \geqslant 31$), very slow electrons can be emitted, and the annihilation of $\bar{p}p$ may be significant before the electron runs away.

In the present energy range, the direct annihilation occurring during the $\bar{p}$ + H collision is important, and should be distinguished from the indirect annihilation of $\bar{p}p$ occurring after the capture process. For the direct annihilation during the collision, only the $J = 0$ wave is important, and the other $J \geqslant 1$ waves have been found negligible. As a result, the point-charge approximation is always very good for the capture probabilities of $J \geqslant 1$. At very low energies, however, the point-charge approximation becomes good also for the capture of $J = 0$. Only in the case that the collision energy is extremely low, can one estimate the direct annihilation probability by using the BO model. The total annihilation cross section $\sigma_{\rm ann}^{\rm tot} = \sigma_{\rm ann} + \sigma_{\rm cap}(L = 0)$ becomes larger than the net capture cross section $\sigma_{\rm cap}^{\rm net} = \sigma_{\rm cap} - \sigma_{\rm cap}(L = 0)$ when $E_{\rm coll} \lesssim 10^{-6}$ eV. The point-charge approximation provides about 80–90% of $\sigma_{\rm ann}^{\rm tot}$ in the present energy range. The 2B annihilation cross section of $\bar{p} + p$ is always larger than $\sigma_{\rm ann}$, but becomes smaller than $\sigma_{\rm ann}^{\rm tot}$ at high energies. This is an interesting finding in understanding plausible processes of $\bar{p}$ annihilation in gases.

The total and N-state selected capture cross sections show an undulation structure which is more pronounced than expected in the quantal Langevin model [52]. At a fixed collision energy, the L-state selected capture cross section becomes the largest for $L \sim J_{\rm orb}$ (the orbiting angular momentum), and is roughly proportional to the statistical weight $(2L + 1)$ for $L \lesssim J_{\rm orb}$. The energetically highest $N = 30$ product state is the most populated in the capture, and the population of this state accounts for about 50% of the total capture.

In a previous study of μ^- + H [26], the calculation was carried out up to a collision energy above the threshold of a higher capture channel. The state-selected cross section for this capture channel rises abruptly from zero at energies just above the threshold, and soon becomes larger than the others when the energy increases only slightly from the threshold. For this reason, the total capture cross section for μ^- + H has a cusp structure around the threshold [55]. The same feature is also expected in the present $\bar{p}$ + H system.

[1] C. J. Batty, Rep. Prog. Phys. **52**, 1165 (1989).
[2] E. Klempt, F. Bradamante, A. Martin, and J. M. Richard, Phys. Rep. **368**, 119 (2002).
[3] D. Gotta, Prog. Part. Nucl. Phys. **52**, 133 (2004).
[4] E. Fermi and E. Teller, Phys. Rev. **72**, 399 (1947).
[5] J. S. Cohen, Rep. Prog. Phys. **67**, 1769 (2004).
[6] D. West, Rep. Prog. Phys. **21**, 271 (1958).
[7] G. B. Andresen *et al.*, Phys. Rev. Lett. **105**, 013003 (2010).
[8] G. Gabrielse *et al.*, Phys. Rev. Lett. **106**, 073002 (2011).
[9] S. Jonsell, A. Saenz, P. Froelich, B. Zygelman, and A. Dalgarno, Phys. Rev. A **64**, 052712 (2001).
[10] A. Yu. Voronin and J. Carbonell, Nucl. Phys. A **689**, 529c (2001).
[11] S. Jonsell, A. Saenz, P. Froelich, B. Zygelman, and A. Dalgarno, J. Phys. B **37**, 1195 (2004).
[12] E. A. G. Armour, Y. Liu, and A. Vigier, J. Phys. B **38**, L47 (2005).
[13] P. Berggren, H. Stegeby, A. Voronin, and P. Froelich, J. Phys. B **41**, 155202 (2008).
[14] G. Gabrielse *et al.*, Phys. Rev. Lett. **89**, 233401 (2002).
[15] M. Amoretti *et al.*, Nature (London) **419**, 456 (2002).
[16] G. B. Andresen *et al.*, J. Phys. B **41**, 011001 (2008).
[17] G. Gabrielse *et al.*, Phys. Rev. Lett. **100**, 113001 (2008).
[18] C. Amole *et al.*, Nature (London) **483**, 439 (2012).
[19] G. Gabrielse *et al.*, Phys. Rev. Lett. **108**, 113002 (2012).
[20] T. L. Trueman, Nucl. Phys. **26**, 57 (1961).
[21] A. Yu. Voronin and J. Carbonell, Phys. Rev. A **57**, 4335 (1998).
[22] K. Sakimoto, Phys. Rev. A **65**, 012706 (2001).
[23] N. Yamanaka and A. Ichimura, Phys. Rev. A **74**, 012503 (2006).
[24] X. M. Tong, K. Hino, and N. Toshima, Phys. Rev. Lett. **97**, 243202 (2006).
[25] P. G. Burke and W. D. Robb, Adv. At. Mol. Phys. **11**, 143 (1976).
[26] K. Sakimoto, Phys. Rev. A **81**, 012511 (2010).
[27] J. C. Light and R. B. Walker, J. Chem. Phys. **65**, 4272 (1976).
[28] J. C. Light, R. B. Walker, E. B. Stechel, and T. G. Schmalz, Comput. Phys. Commun. **17**, 89 (1979).
[29] P. G. Burke, C. J. Noble, and P. Scott, Proc. R. Soc. London, Ser. A **410**, 289 (1987).
[30] M. Le Dourneuf, J. M. Launay, and P. G. Burke, J. Phys. B **23**, L559 (1990).
[31] K. M. Dunseath, M. Le Dourneuf, M. Terao-Dunseath, and J. M. Launay, Phys. Rev. A **54**, 561 (1996).
[32] X. M. Tong and N. Toshima, Phys. Rev. A **85**, 032709 (2012).
[33] K. Sakimoto, Phys. Rev. A **82**, 012501 (2010).
[34] R. F. Walls, R. Herman, and H. W. Milnes, J. Mol. Spectrosc. **4**, 51 (1960).
[35] C. Bloch, Nucl. Phys. **4**, 503 (1957).
[36] P. G. Burke, in *Potential Scattering in Atomic Physics* (Plenum Press, New York, 1977), Chap. 6.
[37] M. J. Seaton, Rep. Prog. Phys. **46**, 167 (1983).
[38] K. V. Protasov, G. Bonomi, E. Lodi Rizzini, and A. Zenoni, Eur. Phys. J. A **7**, 429 (2000).
[39] J. Mitroy and I. A. Ivallov, J. Phys. G **27**, 1421 (2001).
[40] S. G. Karshenboim, Phys. Rep. **422**, 1 (2005).
[41] K. L. Baluja, P. G. Burke, and L. A. Morgan, Comput. Phys. Commun. **27**, 299 (1982).
[42] D. Baye, M. Hesse, J-M. Sparenberg, and M. Vincke, J. Phys. B **31**, 3439 (1998).
[43] A. Igarashi and L. Gulyás, J. Phys. B **42**, 035201 (2009).
[44] J. N. Bardsley and R. K. Nesbet, Phys. Rev. A **8**, 203 (1973).
[45] L. D. Landau and E. M. Lifshitz, *Quantum Mechanics* (Addison-Wesley, Reading, MA, 1958), Sec. 118.
[46] S. Jonsell, E. A. G. Armour, M. Plummer, Y. Liu, and A. C. Todd, New J. Phys. **14**, 035013 (2012).
[47] K. Sakimoto, Phys. Rev. A **66**, 032506 (2002).
[48] F. T. Smith, Phys. Rev. **118**, 349 (1960).
[49] L. I. Schiff, *Quantum Mechanics* (McGraw-Hill, Tokyo, 1968), Sec. 17.
[50] S. C. Miller, Jr. and R. H. Good, Jr., Phys. Rev. **91**, 174 (1953).
[51] W. A. Friedman and C. J. Goebel, Ann. Phys. **104**, 145 (1977).
[52] B. Gao, Phys. Rev. A **83**, 062712 (2011).
[53] G. Gioumousis and D. P. Stevenson, J. Chem. Phys. **29**, 294 (1958).
[54] R. J. Whitehead, J. F. McCann, and I. Shimamura, Phys. Rev. A **64**, 023401 (2001).
[55] R. G. Newton, *Scattering Theory of Waves and Particles* (Springer-Verlag, New York, 1982), Sec. 17.2.